Available online at www.sciencedirect.com
ScienceDirect
International Journal of Heat and Mass Transfer 50 (2007) 3291–3301
International Journal of HEAT and MASS TRANSFER
www.elsevier.com/locate/ijhmt

Jet impingement heat transfer – Part I: Mean and root-mean-square heat transfer and velocity distributions

Tadhg S. O'Donovan *, Darina B. Murray

Department of Mechanical and Manufacturing Engineering, Trinity College Dublin, Ireland

Received 1 August 2006; received in revised form 28 January 2007
Available online 5 April 2007

Abstract

Impinging jets provide a means of achieving high heat transfer coefficients both locally and on an area averaged basis. The current work forms the first stage of a two part investigation of heat transfer distributions from a heated flat surface subject to an impinging air jet for Reynolds numbers from 10,000 to 30,000 and non-dimensional surface to jet exit spacing, H/D, from 0.5 to 8. In the present paper, the relative magnitudes of the local heat transfer coefficients are compared to the fluctuating components and to the mean and root-mean-square local velocity components. It has been shown that at low nozzle to surface spacings (<2 diameters) secondary peaks in the radial heat transfer distributions are due to an abrupt increase in turbulence in the wall jet. In particular the velocity fluctuations normal to the impingement surface have a controlling influence on the enhancement in the wall jet.

Keywords: Jet impingement; Heat transfer; Turbulence

1. Introduction

Impinging jets are known as a method of achieving particularly high heat transfer coefficients and are therefore employed in many engineering applications. Impinging jets have been used to transfer heat in diverse applications, which include the drying of paper and the cooling of turbine blades. Hollworth and Durbin [1] investigated the impingement cooling of electronics, Roy et al. [2] investigated the jet impingement heat transfer on the inside of a vehicle windscreen and Babic et al. [3] used jet impingement for the cooling of a grinding process. In these, and in other cases, research has been conducted with a specific application in mind but there have also been many fundamental investigations into the fluid flow and heat transfer characteristics. These have led to the identification of several parameters which influence heat transfer on the impingement surface. Thus, the main variables for jet impingement heat transfer are the angle of impingement, the jet Reynolds number and the height of the nozzle above the impingement surface. The current investigation is concerned with heat transfer to a submerged normally impinging axially symmetric air jet.

Comprehensive studies of the mean fluid flow characteristics of both a free and an axially symmetric impinging air jet have been presented by Donaldson and Snedeker [4], Beltaos [5] and Martin [6]. In many investigations, including that by Gardon and Akfirat [7], the heat transfer to an impinging jet has been correlated with what is often termed the "arrival" flow condition. This is the flow condition at an equivalent location in a free jet.

Jet flow characteristics are highly complex and can be influenced easily by varying the flow rate and nozzle geometry; the effects of nozzle geometry on the potential core length were investigated by Ashforth-Frost and Jambunathan [8]. Four jet exit conditions were studied, namely flat and fully developed flow for unconfined and semi-confined jets. For unconfined jets, it was shown that the potential core length can be 7% longer for the fully developed flow case.

* Corresponding author. Tel.: +353 1 896 3878; fax: +353 1 679 5554.
E-mail address: tadhg.odonovan@tcd.ie (T.S. O'Donovan).

0017-9310/$ - see front matter © 2007 Elsevier Ltd. All rights reserved.
doi:10.1016/j.ijheatmasstransfer.2007.01.044

Nomenclature

D	diameter [m]
E	electro motive force [V]
h	convective heat transfer coefficient [W/m^2 K]
H	height of nozzle above surface [m]
k	thermal conductivity [W/m K]
Nu	Nusselt number, hD/k [–]
Nu'	root-mean-square Nusselt number [–]
q	rate of heat transfer [W]
q'	root-mean-square heat transfer rate [W]
$\ddot{q}$	heat flux [W/m^2]
r	radial distance from geometric centre [m]
R	resistance [Ω]
Re	jet Reynolds number, $\rho UD/\mu$ [–]
T	temperature [K]
U	velocity [m/s]

Greek symbols

δ	sensor thickness [m]
μ	viscosity [kg/m s]
ρ	density [kg/m^3]

Subscripts

j	jet
max	maximum
s	sensor
stag	stagnation point
surf	surface

Semi-confinement has the effect of reducing entrainment and also elongates the potential core length by up to 20%.

Comprehensive reviews of the heat transfer to impinging jets have been presented by Martin [6], Jambunathan et al. [9] and Polat et al. [10]. The heat transfer distribution to an impinging jet varies significantly in shape and magnitude with the various test parameters.

Goldstein et al. [11] have presented the variation of the stagnation point Nusselt number (Nu_{stag}) with H/D. At nozzle to surface spacings that correspond to impingement within the potential core length, the stagnation point heat transfer is relatively low and constant. Nu_{stag} increases with H/D for distances beyond the potential core length until it reaches a maximum at $H/D = 8$. This increase is attributed to the penetration of turbulence induced mixing from the shear layer to the centreline of the jet. The decrease beyond $H/D = 8$ is due to the lower arrival velocity of the jet. Similar variation of the stagnation point Nusselt number has been reported by Lee et al. [12], however Nu_{max} occurs at $H/D = 6$; the difference between the two studies has been attributed to the different potential core lengths. Ashforth-Frost and Jambunathan [8] have shown that the maximum stagnation point Nusselt number occurs at a distance from the nozzle exit of approximately 110% of the potential core length. At this location the enhanced heat transfer due to increased turbulence intensity more than compensates for the loss of centreline velocity. Semi-confinement has been shown to reduce the stagnation point heat transfer by up to 10% at the optimal H/D. This is due to the lower level of turbulence because of reduced entrainment. Hoogendoorn [13] reported on the heat transfer distribution in the vicinity of the stagnation point. For a jet issuing with a low turbulence intensity (<1%) the stagnation point heat transfer is a local minimum for $H/D \leqslant 4$. This is not the case for a jet that has high mainstream turbulence ($\geqslant 5\%$), where the peak in the heat transfer distribution occurs at the stagnation point.

The shape of the radial heat transfer distribution is affected by the height of the nozzle above the impingement surface. Several investigators, including Donaldson and Snedeker [14], Goldstein and Behbahani [15] and others presented heat transfer data for a jet impinging at large H/D. According to Mohanty and Tawfek [16] the heat transfer rate peaks at the stagnation point and decreases exponentially with increasing radial distance beyond $r/D = 0.5$ for a relatively large range of nozzle to impingement surface spacings ($4 < H/D < 58$).

In studies by Baughn and Shimizu [17], Huang and El-Genk [18], Goldstein et al. [11] and others, secondary peaks in the heat transfer distribution to an impinging air jet have been reported. In some cases two radial peaks are present in the heat transfer distributions. Both Hoogendoorn [13] and Lytle and Webb [19] have proposed that at low H/D, the wall jet boundary layer thickness decreases with distance from the stagnation point as the flow escapes through the minimum gap between the nozzle lip and the impingement surface. In the case of a low turbulence jet this thinning results in a local maximum in the heat transfer distribution. With further increase in distance from the stagnation point the laminar boundary layer thickness increases before transition to a fully turbulent flow. Effectively the thickening of the laminar boundary layer decreases the rate of heat transfer and upon transition to a fully turbulent wall jet, the heat transfer distribution increases to a secondary peak.

Goldstein and Timmers [20] compared heat transfer distributions of a large nozzle to plate spacing ($H/D = 6$) to that of a relatively small spacing ($H/D = 2$). This study had a uniform wall flux thermal boundary condition. It was shown that while the Nusselt number decays from a peak at the stagnation point for the large H/D, the Nusselt number is a local minimum at the stagnation point when $H/D = 2$. Overall, for the same jet Reynolds number the heat transfer coefficient is lower for the lower H/D. This

is attributed to the fact that the mixing induced in the shear layer of the jet has not penetrated to the potential core of the jet. The flow within the potential core has relatively low turbulence and consequently the heat transfer is lower in this case. Although not discussed, it is apparent from the results presented by Goldstein and Timmers [20] that subtle peaks occur at a radial position.

Goldstein et al. [11] continued research in this area. This investigation concentrated on a wider range of nozzle to plate spacings ($2 \leqslant H/D \leqslant 10$) and Reynolds numbers ($60{,}000 < Re < 124{,}000$). Once again at small spacings, $H/D \leqslant 5$, secondary maxima are evident at a radial location in the heat transfer distribution. In the case where $H/D = 2$ these maxima are greater than the stagnation point Nusselt number. The secondary maxima occur at a radial distance of approximately 2 diameters from the stagnation point and were attributed to entrained air caused by vortex rings in the shear layer.

The current investigation presents data for the most common nozzle type found in the literature, i.e. a hydrodynamically fully developed jet that issues from a long pipe. Mean and fluctuating heat transfer distributions from a heated surface to the impinging air jet are compared with local velocity measurements. The literature to date has shown that the heat transfer to an impinging air jet is highly sensitive to each of the many experimental parameters that exist. The shape of the heat transfer distribution in particular varies considerably with height of the jet nozzle above the impingement surface. Of particular interest to the current investigation are the secondary peaks that occur in the mean heat transfer distribution when the jet nozzle is placed within 2 diameters of the impingement surface. While abrupt increases in turbulence in the wall jet are used to explain the location and magnitude of secondary peaks in heat transfer the literature fails to provide an in depth explanation of the mechanism responsible. It has been shown that for the range of $H/D \leqslant 2$ the magnitude of the turbulence in the wall jet does not change significantly. The magnitude of the secondary peaks in heat transfer varies considerably within this range however. An important objective of the current research therefore is to investigate the turbulent fluctuations within the wall jet in order to reveal the fluid flow and convective heat transfer mechanisms that influence the magnitude and location of these peaks. The current paper correlates peaks in local velocity components with enhanced heat transfer coefficients. A temporal investigation of both the heat transfer and the fluid velocity close to the surface is presented in a companion paper where the effect of vortices on heat transfer is presented.

2. Experimental rig

The main elements of the experimental rig are a nozzle and an impingement surface (Fig. 1). Both are mounted on independent carriages that travel on orthogonal tracks. The flat impingement surface is instrumented with two single point heat flux sensors and the ability of the carriages to move in this way enables the jet to be positioned relative to the sensors at any location in a two dimensional plane. The heated flat plate consists of three main layers, measuring 425 mm × 550 mm. The top surface is a 5 mm thick copper plate. A silicon rubber heater mat, approximately 1.1 mm thick, is fixed to the underside of the copper plate with a thin layer of adhesive. It has a power rating of 15 kW/m^2 and a voltage rating of 230 V. The voltage is varied using a variable transformer that controls the heat supplied to the copper plate. A thick layer of insulation prevents heat loss from the heating element other than through the copper. The plate assembly is such that it approximates a uniform wall temperature boundary condition, operating typically at a surface temperature of 60 °C. The maximum

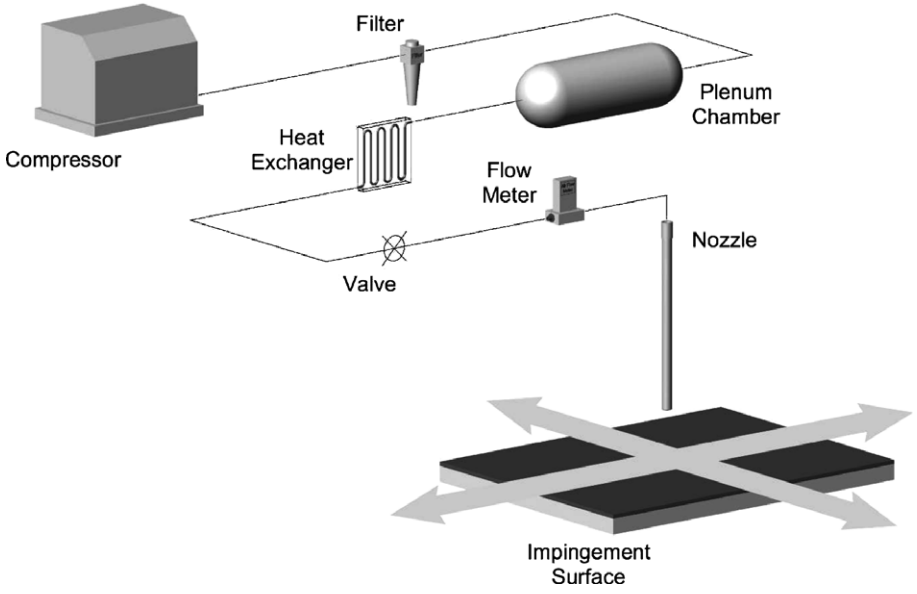

Fig. 1. Experimental rig.

temperature gradient across the impingement surface during testing was measured to be 5 °C. The heat transfer coefficient is calculated from accurately measured local surface temperature and heat flux measurements. This small deviation from a uniform wall temperature boundary condition is taken into consideration in the interpretation of results.

The nozzle consists of a brass pipe of 13.5 mm internal diameter. The pipe is 20 diameters long and a 45° chamfer is machined at the nozzle lip to create a sharp edge to minimise entrainment. The resulting flow that issues from the nozzle has been shown by O'Donovan [21] to be a fully developed turbulent jet. The nozzle is clamped on a carriage in an arrangement that allows its height above the impingement surface to be varied, with a range from 0.5 to 8 nozzle diameters above the impingement surface.

Air is supplied to the jet nozzle by a compressor. An Alicat Scientific Inc. Precision Gas Flow Meter is installed on the compressed air line to monitor both the air volume flow rate and temperature. Real time acquisition of the air volume flow rate allows for accurate setting of the jet exit Reynolds number, by varying a needle control valve also installed on the line, just prior to the flow meter. For this investigation the jet exit temperature is maintained within 0.5 °C of the ambient air temperature by using a heat exchanger installed on the air line.

Two sensors are flush mounted on the heated impingement surface. These are an RdF Micro-Foil® heat flux sensor and a Senflex® Hot Film Sensor. T-type thermocouples are also placed on the instrumented plate in the vicinity of the two heat flux sensors to measure the surface temperature locally. Finally, a thermocouple is placed in the jet flow line at the flow meter and another in the ambient air near the nozzle exit to monitor the entrained air temperature.

The RdF Micro-Foil® heat flux sensor consists of a differential thermopile that measures the temperature above and below a known thermal barrier. The heat flux through the sensor is therefore defined by Eq. (1).

$$\ddot{q} = k_s \frac{\Delta T}{\delta} \tag{1}$$

where k_s is the thermal conductivity of the barrier (kapton) and ΔT is the temperature difference across the thickness (δ) of the barrier. A single pole thermocouple is also embedded in this sensor to measure the surface temperature locally. For the specific sensor used the characteristic 62% response to a step function is 0.02 s.

The Senflex® hot film sensor operates in conjunction with a Constant Temperature Anemometer to measure the fluctuating heat flux to the impinging jet, as it has higher temporal resolution than the Micro-Foil® sensor and can accurately acquire data in excess of 8 kHz. This equates to a Nyquist frequency of 4096 Hz and for the maximum jet exit velocity investigated, the Strouhal number is calculated to be approximately 5. This upper value was not required however as the maximum Strouhal number associated with coherent structures within the impinging jet flow is less than 2. The sensor consists of a nickel sensor element that is electron beam deposited onto a 0.051 mm thick Upilex S polyimide film. The hot film element has a thickness of <0.2 μm and covers an area of approximately 0.1 mm × 1.4 mm. The typical cold resistance of the sensor is between 6 and 8 Ω.

A TSI Model 1053B Constant Temperature Anemometer is used to control the temperature of the hot film; it maintains the temperature of the film at an overheat (≈5 °C) above the heated surface. The power required to maintain this temperature is equal to the heat dissipated from the film. Thus, the voltage required to maintain the temperature of the film constant is proportional to the heat transfer to the air jet, as described by Eq. (2). The constant of proportionality accounts for losses, including conduction to the impingement surface.

$$q_{\text{dissipated}} \propto \frac{E_{\text{out}}^2}{R} \tag{2}$$

Both the RdF Micro-Foil® heat flux sensor and the Senflex® hot film sensor were calibrated in situ against a reference stagnation point heat transfer coefficient presented by Shadlesky [22]. The calibration of the sensors compared favourably with that provided by the manufacturer's specification.

Laser Doppler Anemometry is employed as a non-intrusive method of measuring the flow velocity close to the impingement surface. Food grade poly-functional alcohol liquid seeding particles, typically 1 to 50 μm in diameter were used to seed both the jet flow and the ambient air. The Laser Doppler Anemometry system is based on a Reliant 500 mW Continuous Wave laser from Laser Physics. This is a two component system and therefore the laser is split into 2 pairs of beams, that have wavelengths of 514.5 nm (green) and 488 nm (blue), to measure the velocity in orthogonal directions at the same point location. The four beams, each of diameter 1.35 mm, are focused on a point 250 mm from the laser head. The system works in backscatter mode and a Base Spectrum Analyser (BSA) acquires and processes the signal to compute the velocity.

Heat transfer results are presented as distributions of the time averaged mean Nusselt number (Nu) and fluctuating Nusselt number (Nu'). The magnitude of the fluctuations of the Nusselt number (Nu') is the root-mean-square (rms) of the Nusselt number signal. The mean and fluctuating Nusselt numbers have calculated uncertainties of 5.7% and 30.0% respectively and are based on the local heat transfer coefficient that is defined by Eq. (3)

$$h(r) = \frac{\ddot{q}(r)}{(T_{\text{surf}}(r) - T_j)} \tag{3}$$

where $\ddot{q}$ is the heat flux signal from the surface, T_j is the jet exit temperature and T_{surf} is the local surface temperature. These uncertainties are based on a worst case scenario where the uncertainty is a percentage of the smallest measurements. It is clear from the results presented that the uncertainty in Nu' is, in general, less than 30%. A complete

calibration and uncertainty analysis for this experimental set-up is presented by O'Donovan [21].

3. Results and discussion

The results from fluid flow and heat transfer measurements of an impinging air jet are presented and analysed in this section. The fluid flow measurements include two components of the fluid velocity close to the surface in a jet impingement configuration. The heat transfer measurements consist mainly of heat transfer distributions over the impingement surface subject to the jet. Results are analysed on both a time averaged and temporal basis.

As detailed in Section 1, there are many parameters that affect the heat transfer to an impinging jet including confinement, submergence, nozzle geometry, non-dimensionalised nozzle to impingement surface spacing (H/D) and jet exit Reynolds number (Re). In the current investigation the influence of confinement, submergence and nozzle geometry have not been investigated. Results are presented for an unconfined air jet issuing from a long pipe for three Reynolds numbers ($Re = 10{,}000,\ 20{,}000,\ 30{,}000$) and six different spacings above the impingement surface, ($H/D = 0.5, 1, 2, 4, 6, 8$). This range of spacings gives good precision at low spacings and extends beyond the potential core length of the jet at the highest Reynolds number. Additional, limited data were also included for some intermediate values of H/D.

The time averaged surface heat transfer data include mean and root-mean-square Nusselt number distributions for the various jet impingement configurations. Nu is based on the heat flux ($\ddot{q}$) and the temperature difference (ΔT) between the jet exiting the nozzle and the impingement surface. Nu' is based on the same temperature difference and the fluctuating heat flux determined by the hot film sensor (q'). Heat transfer data are presented for a zone extending from the geometric centre to a radial distance of 6 diameters.

Three zones can be identified in an impinging jet flow. These are illustrated in Fig. 2. Firstly there is the free jet zone, which is the region that is largely unaffected by the presence of the impingement surface; this exists beyond approximately 1.5 diameters from the impingement surface. A potential core exists within the free jet region, within which the jet exit velocity is conserved and the turbulence intensity level is relatively low. A shear layer exists between the potential core and the ambient fluid where the turbulence is relatively high and the mean velocity is lower than the jet exit velocity. The shear layer entrains ambient fluid and causes the jet to spread radially. Beyond the potential core the shear layer has spread to the point where it has penetrated to the centreline of the jet. At this stage the centreline velocity decreases and the turbulence intensity increases. Fig. 2 also identifies a stagnation zone that extends to a radial location defined by the spread of the jet. The stagnation zone includes the stagnation point where the mean velocity is zero and within this zone the free jet is deflected into the wall jet flow. Finally, the wall jet zone extends beyond the radial limits of the stagnation zone.

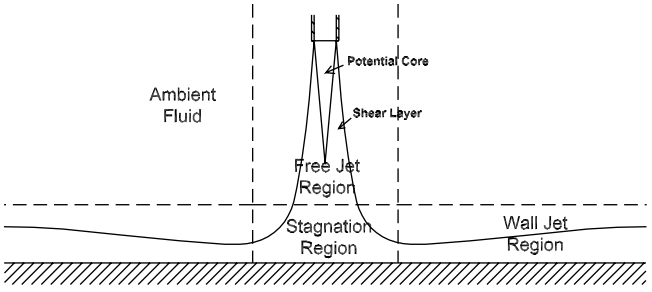

Fig. 2. Impinging jet zones.

3.1. Nusselt number distributions

The measured heat transfer distributions vary considerably with H/D. Distributions for two different heights ($H/D = 0.5; 6.0$) are presented in Fig. 3. These two heights correspond respectively to well within the potential core ($H/D = 0.5$) where the jet exit velocity is conserved across the entirety of the profile, and to a height where the impingement surface is beyond the potential core ($H/D = 6.0$). In the latter case the shear layer has penetrated to the centreline of the jet, resulting in a diminished centreline velocity and in a centreline turbulence intensity which is relatively high.

For the range of parameters tested the Nusselt number distributions exhibit a maximum at the stagnation point. The flow at this point is not truly stagnant in that velocity fluctuations in the radial direction occur, but can be considered stagnant on a time averaged basis. Thus, the mixing that occurs results in the continued introduction of cold fluid, maintaining a high local temperature difference. The combined effects of a high instantaneous velocity and

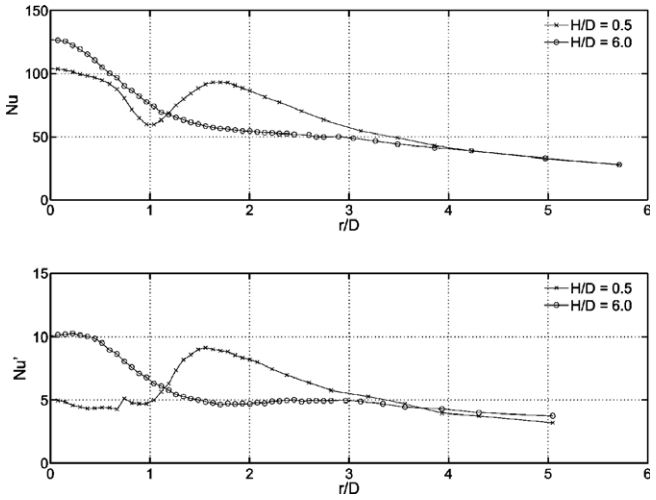

Fig. 3. Radial heat transfer distributions; $Re = 30{,}000$.

large temperature difference results in a heat transfer peak at the stagnation point. At H/D of 0.5, the radial distribution of Nusselt number decreases initially from this maximum but rises again to give a peak at a radial location of $r/D = 1.6$; this location has been found to be both Reynolds number and H/D dependent. Beyond this peak the heat transfer distribution decays with increasing radial distance from the stagnation point. It is thought that these secondary peaks are a result of transition to turbulence of the wall jet boundary layer.

The fluctuating heat transfer distribution, also shown in Fig. 3, is an indication of the instability in the flow along the impingement surface. At $H/D = 0.5$, the free jet exerts pressure on the wall jet within the stagnation zone. This maintains the heat transfer fluctuations low and constant. As the wall jet escapes from the effects of the free jet, it is free to undergo transition to turbulent flow and the combination of high local velocity and turbulence intensity leads to peaks in both the time averaged and fluctuating Nusselt number distributions. This occurs at $r/D = 1.6$. However, the ever increasing local air temperature and the decreasing local fluid velocity eventually negate the effects of high turbulence in the wall jet and the Nusselt number falls off with increasing radial distance. The fluctuations in heat transfer also decrease in magnitude as the local fluid velocity decreases.

At $H/D = 6$ (also shown in Fig. 3) the heat transfer decreases from a peak at the geometric centre with increasing radial distance. At this distance of the nozzle above the plate, the shear layer has penetrated to the centre of the jet and therefore the flow at the geometric centre is highly turbulent. The fluctuations in heat transfer are also a maximum at the stagnation point. The flow velocity along the plate increases from zero at the geometric centre, as the free jet joins the wall jet flow. With further increase in radial distance the wall jet velocity decays as the flow spreads radially. Also at greater radial distances the fluctuations in the flow decrease and the local air temperature increases. This combination of factors results in the heat transfer distribution decaying from a maximum at the geometric centre with increasing radial distance. The fluctuating heat transfer distribution exhibits a subtle secondary peak (at $r/D \approx 3$), indicating that even at this large H/D the free jet remains an influence on the wall jet beyond the potential core length. This is not sufficient to overcome the effects of decreasing radial velocity and decreasing local temperature difference, however, so that the time averaged Nusselt number continues to fall.

Studies by Goldstein and Behbahani [15], and others have shown the Nusselt number at the stagnation point to be a local minimum. This is the case where the Reynolds number is very high and/or the nozzle to plate spacing is extremely low and is true for a low turbulence jet only. In these circumstances the flow genuinely does stagnate and therefore the heat transfer is low.

Time averaged and fluctuating heat transfer distributions for a much wider range of parameters are plotted in Figs. 4 and 5 respectively. In general, the area averaged heat transfer is greater for higher Re. It is also apparent that as the height of the jet above the plate increases the secondary peaks decrease in magnitude until they eventually disappear. Sec-

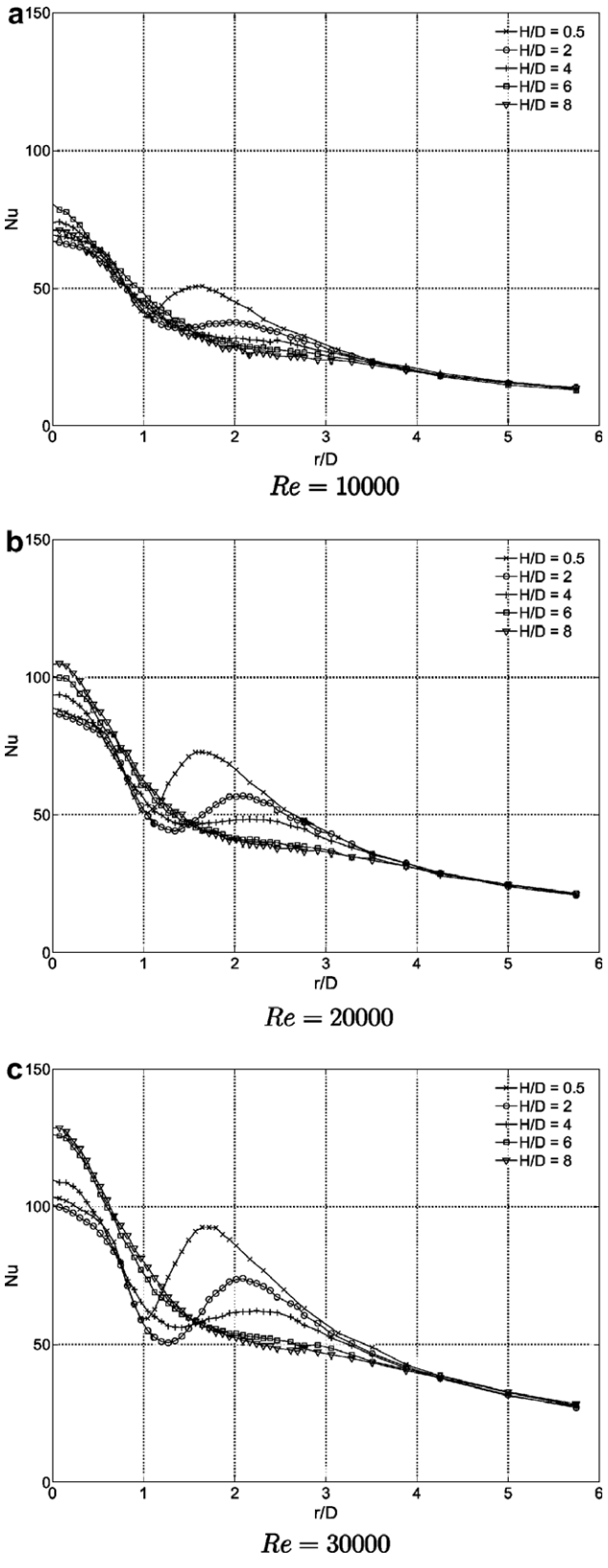

Fig. 4. Time averaged Nusselt number distributions.

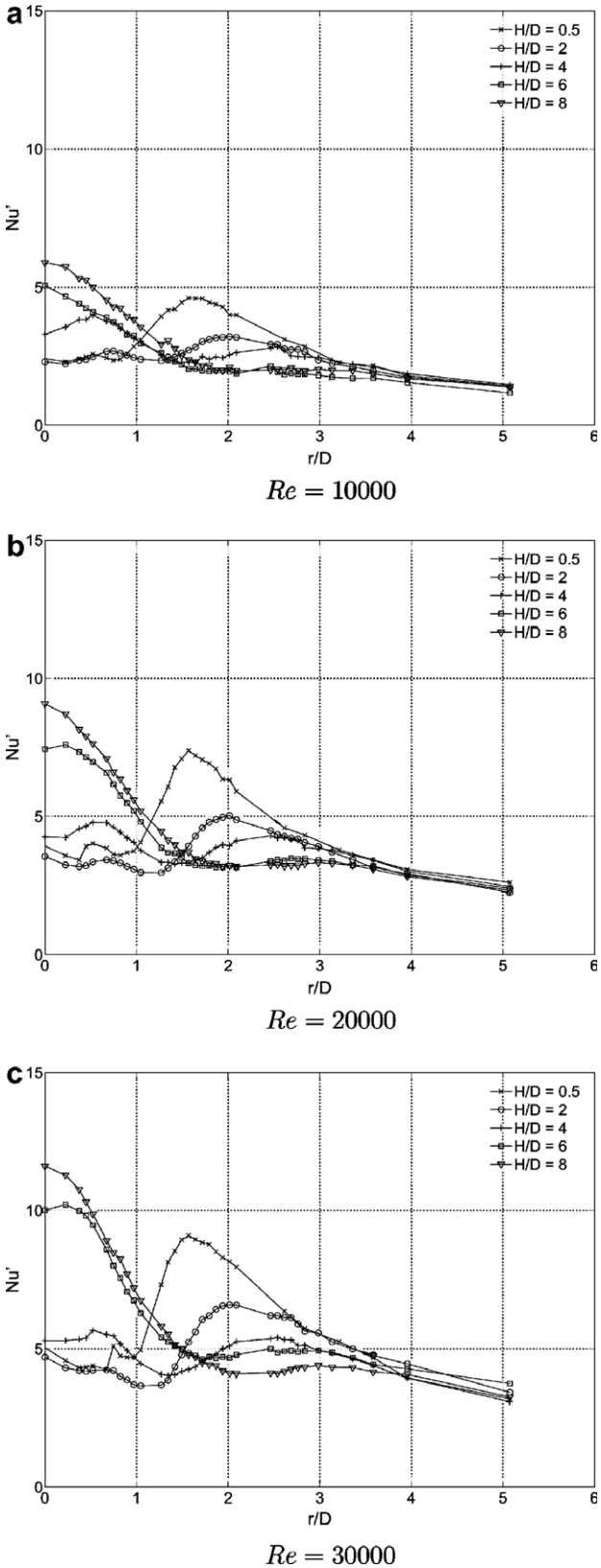

Fig. 5. Fluctuating Nusselt number distributions.

ondary peaks occur at low H/D in both Nu and Nu' distributions, however the highest spacing at which they occur is Reynolds number dependent. This is, in part, due to the elongation of the potential core at larger jet exit velocities.

The area averaged Nu' also increases with Re, as evident from Fig. 5. The distribution, however, has three distinct patterns that are dependent on H/D. An example of each distribution is presented in Fig. 6, together with a schematic representation of its location within the free jet. At very low H/D, as discussed previously, the heat transfer fluctuations are low within the stagnation zone, increasing to a peak and then decreasing as the jet spreads radially. The axial velocity is high and therefore suppresses the fluctuations in the stagnation region. The spread of the jet is also small and therefore once the wall jet has escaped the lip of the jet the heat transfer fluctuations increase rapidly.

At intermediate heights ($2 \leqslant H/D \leqslant 4$) the fluctuations remain low at the stagnation point, however two peaks are evident in the Nu' distribution. In this case the width of the potential core is less and the suppressive nature of the free jet flow is mainly felt across this reduced area. The first peak is located within the shear layer of the free jet and is due to the high turbulence injected into the wall jet flow upon impingement. This peak is much smaller at lower H/D because the shear layer is much narrower. With increasing height this peak moves towards the geometric centre as the shear layer penetrates the core of the jet. The second peak ($r/D = 2$) is once again attributed to the wall jet escaping beyond the constraining effect of the free jet flow. Throughout the range of H/D investigated, this increase in heat transfer does not occur immediately upon escape of the free jet flow; this delay is investigated further in Section 3.2. The jet has spread further at greater H/D and therefore the location of this secondary peak moves further from the

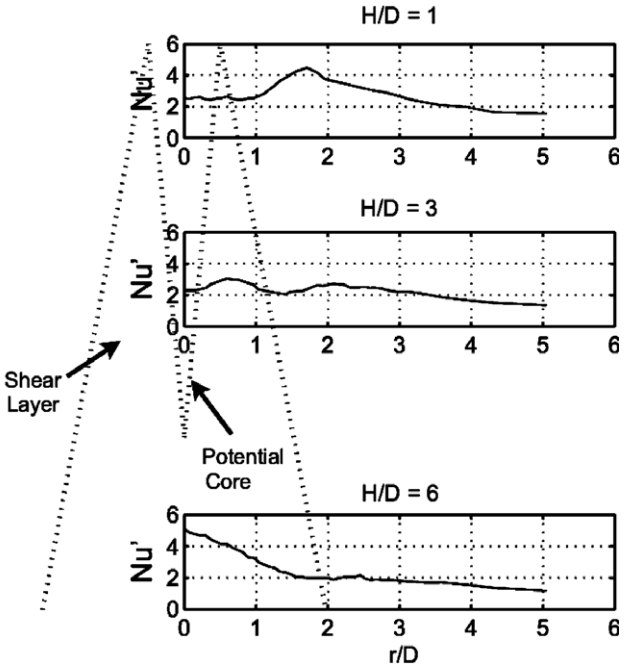

Fig. 6. Nu' distributions; $Re = 10{,}000$.

geometric centre. This can be seen from a comparison of the results for H/D of 2 to 4 in Fig. 5.

The final trend is evident at large H/D, where the potential core width has decreased to zero as evident in Fig. 6 for $H/D = 6$. At this stage the inner peak in the Nu' distribution has reached the geometric centre. This corresponds to the shear layer penetrating to the centreline of the jet. The outer peak has decreased significantly in magnitude at this stage as the axial velocity of the free jet is reduced. In this case the Nu' distribution simply decays from a peak at the stagnation point with increasing radial distance. Evidence in support of this explanation is presented in Section 3.2 where the local flow velocities are qualitatively compared to the heat transfer distributions.

3.2. Heat transfer and velocity measurements

This section qualitatively compares time averaged heat transfer distributions with local velocity data obtained using LDA. Thus, peaks and troughs in the Nu and Nu' distributions are linked to regions of high local fluid velocity and turbulence intensity.

Figs. 7 and 8 compare the flow velocities near the impingement surface to the heat transfer from the surface with a normally impinging jet at H/D of 1 and 8 respectively. Both the axial and the radial velocity components (perpendicular and parallel to the impingement surface respectively) are presented. These measurements were made at a distance of 3 mm from the impingement surface, which was the closest possible given experimental constraints. The abrupt changes in velocity evident in Fig. 7 contribute to the non-monotonic decay of the Nusselt number from a peak at the stagnation point. The axial velocity is a maximum in the stagnation zone; this is often termed the arrival velocity. With increasing radial distance from the stagnation point the axial velocity decreases and may even turn negative (i.e. in a direction away from the impingement surface). The radial velocity is zero at the centreline of the jet which corresponds to the stagnation point. This velocity increases initially with increasing distance from the stagnation point but peaks at a radial location ($r/D \approx 0.7$) beyond the lip of the jet as the jet spreads radially.

Fig. 7 demonstrates that at low H/D the axial velocity profile is more uniform for the region defined by $r/D < 0.5$ than in the case where $H/D = 8$, which is presented in Fig. 8. This indicates that the surface is within the potential core of the jet at $H/D = 1$. It can also be seen from a comparison of the root-mean square velocities for both H/D that a high stagnation region axial velocity suppresses fluctuations in the wall jet flow. The effect of the mean and rms velocities on the mean and fluctuating heat transfer is also apparent in both figures. At $H/D = 1$ the axial velocity magnitude decays sharply beyond $r/D = 0.5$ and once this axial velocity has decreased sufficiently the wall jet flow is less constrained and undergoes transition to a highly turbulent flow. Both the radial and axial rms velocity distributions exhibit peaks at radial locations where the axial velocity is low. Lytle and Webb [19] have shown, for $H/D \leqslant 1$, that a peak in velocity fluctuations parallel with the impingement surface corresponds to a peak in the mean heat transfer distribution. The current research concurs with this. However the current study shows that at greater values of H/D the peaks in rms velocity, for the axial velocity in particular, correspond in location to peaks in both the mean and fluctuating heat transfer

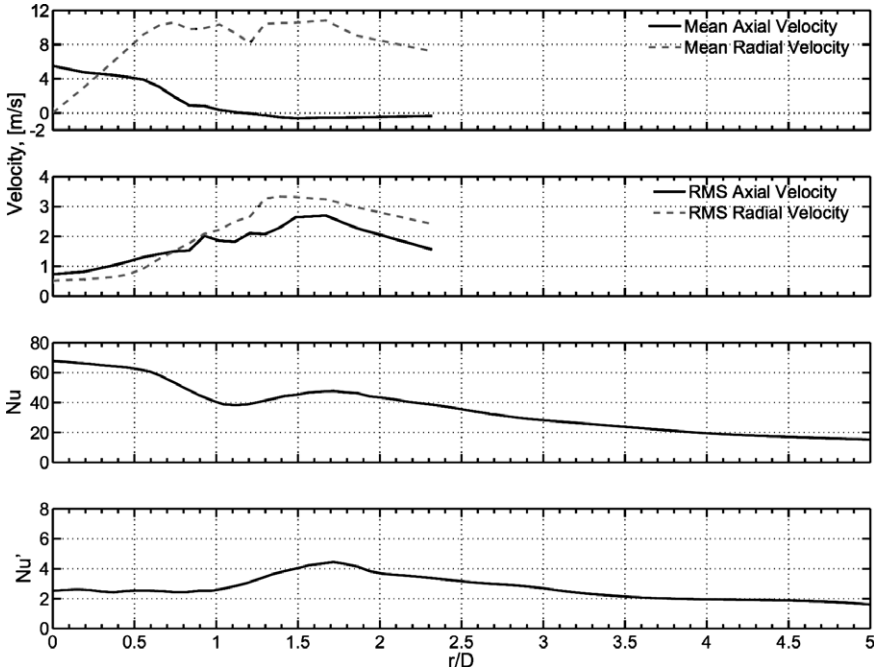

Fig. 7. Flow velocity and heat transfer; $Re = 10{,}000$, $H/D = 1$.

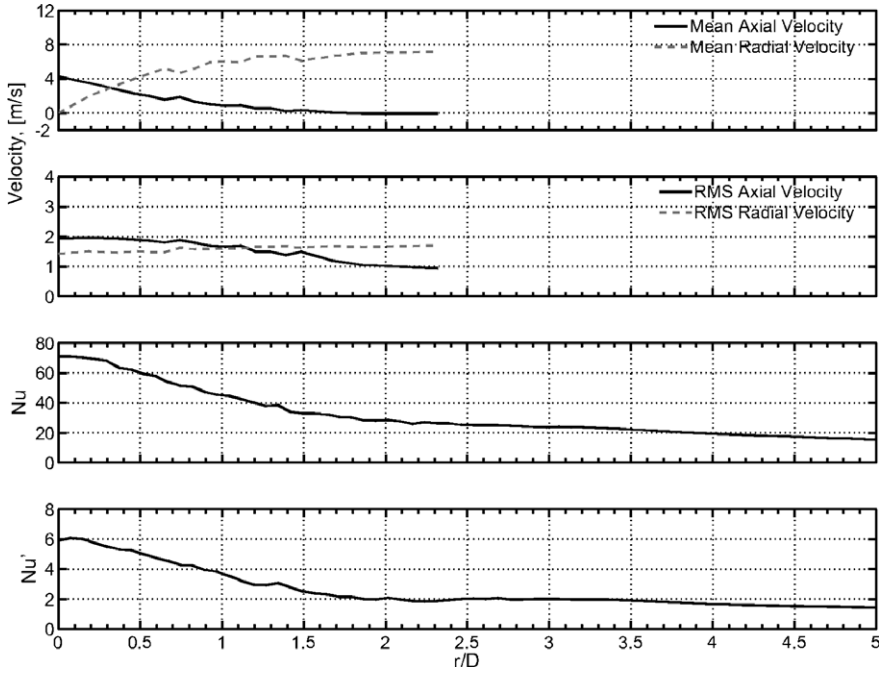

Fig. 8. Flow velocity and heat transfer; $Re = 10{,}000$, $H/D = 8$.

distributions as seen in Fig. 9. At larger H/D, as indicated in Fig. 8, the axial velocity has a much smaller magnitude in the region $r/D < 1$ and therefore does not have the same suppressive effect on the development of the wall jet flow. As a result the entire profile has a more uniform turbulence level and peaks are not evident in either the mean or fluctuating heat transfer distributions.

From Fig. 7 the secondary peak in the Nu distribution at $H/D = 1$ occurs at the same radial location as the peak in the Nu' distribution. Fig. 9 depicts the location of the peaks in both the Nu and Nu' distributions for a range of jet to plate spacings and jet Reynolds numbers and compares them to the location of the peaks in both rms axial and radial velocities. As was shown in Fig. 4, the Nusselt number distributions continue to exhibit secondary peaks up to a nozzle to plate spacing which depends on the jet Reynolds number. The radial location of the peak, however, is independent of the Reynolds number but moves in the positive radial direction as H/D increases. A similar trend is evident for the peak locations in the Nu' distributions, as shown in Fig. 9b. The fact that the peaks occur at the same location for both Nu and Nu' distributions indicates a correlation between the heat transfer fluctuations and the mean heat transfer. In general, fluctuations in the local

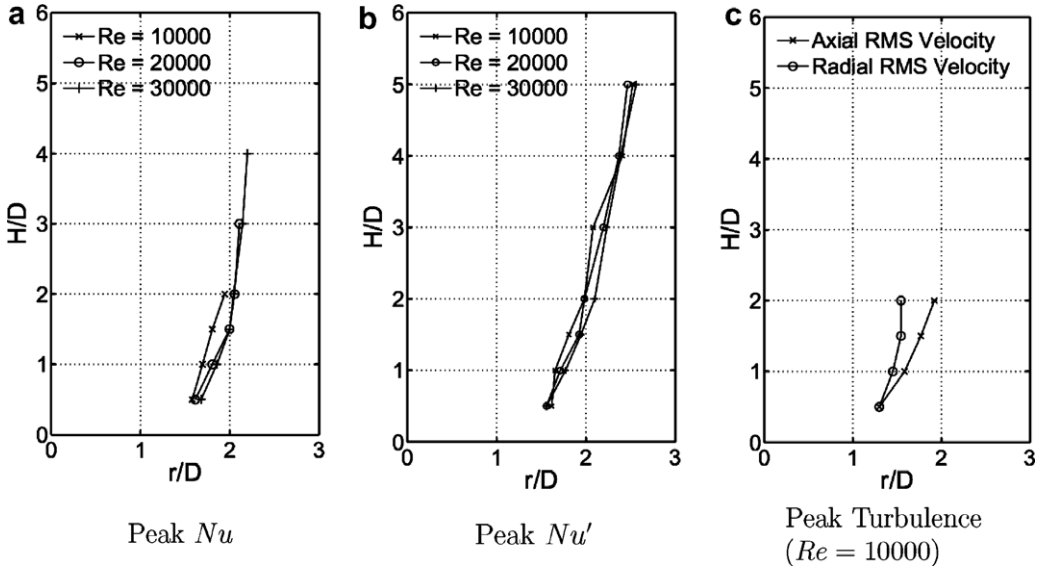

Fig. 9. Location of heat transfer maxima and maximum turbulence intensity.

flow velocity will have the effect of enhancing both the mean and the fluctuating heat transfer. However, the fact that the peaks in the Nu' distribution (Fig. 9b) are evident at nozzle to plate spacings for which there are no peaks in the mean Nusselt number distribution (Fig. 9a) indicates that other factors must influence the mean heat transfer.

As the location of the heat transfer peaks moves radially outwards with increasing H/D it is hypothesised that this is due to the spreading of the free jet flow. Previous studies by Gardon and Akfirat [7] have related the flow characteristics of a free jet to the heat transfer characteristics for a similar jet in an impingement configuration. A more relevant comparison has been achieved in this study with the use of the local fluid velocities along the surface subject to the jet impingement. The location of the peak in the local turbulence intensity is presented in Fig. 9c. For $H/D > 2$ no peaks were evident in the turbulence intensity profiles. Also, as the height of the nozzle above the impingement surface increases a divergence between the locations of the peak radial and axial velocity fluctuations is realised. The peak in Nusselt number occurs close to the peak in the axial velocity fluctuation and therefore it is surmised that the heat transfer is dependent primarily on the magnitude of fluctuations in velocity normal to the surface. Data presented by Lytle and Webb [19] were limited to mean heat transfer distributions and velocity fluctuations parallel with the impingement surface. Therefore for their low H/D range the correlation between high radial velocity fluctuations and a peak in the mean heat transfer is valid. The current research has shown that this cannot be extrapolated for a larger range of H/D. Analysis of the coherence between the surface heat flux and local velocity signals will reveal the extent to which vertical velocity fluctuations influence heat transfer. These data will be presented in a companion paper. It will also consider the effect that naturally occurring vortices have on jet impingement heat transfer.

4. Conclusions

Results have been presented of fluid flow and heat transfer relating to an axially symmetric impinging air jet. It has been shown that at low nozzle to impingement surface spacings the mean heat transfer distribution in the radial direction exhibits secondary peaks. These peaks have been reported by several investigators and have been attributed, in general, to an abrupt increase in turbulence in the wall jet boundary layer. Results from the current investigation support this assertion.

Although the link between heat transfer peaks and turbulence has been established, the fluid mechanical processes that control the turbulence level in the wall jet have not been well defined. It has been shown here that the free jet flow has the effect of suppressing turbulence in the wall flow, and upon 'escaping' from the lip of the free jet the wall jet can undergo transition to a fully turbulent flow; this transition to turbulence does not occur immediately after the wall jet escapes the free jet flow, however. Further work must include analysis of the fluctuating component of both axial and radial velocity signals as well as the heat transfer signal. This is presented in the second part of this investigation.

It has been shown also that the magnitude of the secondary peak in the Nusselt number distribution is influenced more by velocity fluctuations normal to the surface than by fluctuations parallel with the surface. This is consistent with the direction of the maximum temperature gradient. What remains unclear is why velocity fluctuations in different directions vary in magnitude in this way. Further analysis of the fluctuating velocity and heat transfer signals in the companion paper addresses this issue and thereby contributes to the understanding of the overall heat transfer characteristics.

Acknowledgement

This work was supported in part by Enterprise Ireland under grant SC/2001/0071 and also by Science Foundation Ireland grant 04/BR/EO108.

References

[1] B.R. Hollworth, M. Durbin, Impingement cooling of electronics, ASME J. Heat Transfer 114 (1992) 607–613.
[2] S. Roy, K. Nasr, P. Patel, B. AbdulNour, An experimental and numerical study of heat transfer off an inclined surface subject to an impinging airflow, Int. J. Heat Mass Transfer 45 (2002) 1615–1629.
[3] D.M. Babic, D.B. Murray, A.A. Torrance, Mist jet cooling of grinding processes, Int. J. Mach. Tools Manuf. 45 (2005) 1171–1177.
[4] C.D. Donaldson, R.S. Snedeker, A study of free jet impingement part i mean properties of free impinging jets, J. Fluid Mech. 45 (1971) 281–319.
[5] S. Beltaos, Oblique impingement of circular turbulent jets, J. Hydraul. Res. 14 (1976) 17–36.
[6] H. Martin, Heat and mass transfer between impinging gas jets and solid surfaces, Adv. Heat Transfer 13 (1977) 1–60.
[7] R.J. Gardon, J.C. Akfirat, The role of turbulence in determining the heat transfer characteristics of impinging jets, Int. J. Heat Mass Transfer 8 (1965) 1261–1272.
[8] S. Ashforth-Frost, K. Jambunathan, Effect of nozzle geometry and semi-confinement on the potential core of a turbulent axisymmetric free jet, Int. Commun. Heat Mass Transfer 23 (1996) 155–162.
[9] K. Jambunathan, E. Lai, M.A. Moss, B.L. Button, A review of heat transfer data for a single circular jet impingement, Int. J. Heat Fluid Flow 13 (1992) 106–115.
[10] S. Polat, B. Huang, A.S. Mujumdar, W.J.M. Douglas, Numerical flow and heat transfer under impinging jets: a review, Annu. Rev. Numer. Fluid Mech. Heat Transfer 2 (1989) 157–197.
[11] R.J. Goldstein, A.I. Behbahani, K. Heppelmann, Streamwise distribution of the recovery factor and the local heat transfer coefficient to an impinging circular air jet, Int. J. Heat Mass Transfer 29 (1986) 1227–1235.
[12] D.H. Lee, R. Grief, S.J. Lee, J.H. Lee, Heat transfer from a plate to a fully developed axisymmetric impinging jet, ASME J. Heat Transfer 117 (1995) 772–776.
[13] C.J. Hoogendoorn, The effect of turbulence on heat transfer at a stagnation point, Int. J. Heat Mass Transfer 20 (1977) 1333–1338.
[14] C.D. Donaldson, R.S. Snedeker, D.P. Margolis, A study of free jet impingement part. ii. free jet turbulent structure and impingement heat transfer, J. Fluid Mech. 45 (1971) 477–512.

[15] R.J. Goldstein, A.I. Behbahani, Impingement of a circular jet with and without cross flow, Int. J. Heat Mass Transfer 25 (1982) 1377–1382.
[16] A.K. Mohanty, A.A. Tawfek, Heat transfer due to a round jet impinging normal to a flat surface, Int. J. Heat Mass Transfer 36 (1993) 1639–1647.
[17] J.W. Baughn, S.S. Shimizu, Heat transfer measurements from a surface with uniform heat flux and an impinging jet, ASME J. Heat Transfer 111 (1989) 1096–1098.
[18] L. Huang, M.S. El-Genk, Heat transfer of an impinging jet on a flat surface, Int. J. Heat Mass Transfer 37 (1994) 1915–1923.
[19] D. Lytle, B.W. Webb, Air jet impingement heat transfer at low nozzle-plate spacings, Int. J. Heat Mass Transfer 37 (1994) 1687–1697.
[20] R.J. Goldstein, J.F. Timmers, Visualisation of heat transfer from arrays of impinging jets, Int. J. Heat Mass Transfer 25 (1982) 1857–1868.
[21] T.S. O'Donovan, Fluid flow and heat transfer of an impinging air jet, Ph.D. thesis, Department of Mechanical & Manufacturing Engineering, Trinity College Dublin, 2005.
[22] P.S. Shadlesky, Stagnation point heat transfer for jet impingement to a plane surface, AIAA J. 21 (1983) 1214–1215.